The Predictive Power of Computational Astrophysics as a Discovery Tool
Proceedings IAU Symposium No. 362, 2023
D. Bisikalo, D. Wiebe & C. Boily, eds.
doi:10.1017/S1743921322001892

Simulating star formation in spiral galaxies

Steven Rieder[1,2], Clare Dobbs[2], Thomas Bending[2], Kong You Liow[2] and James Wurster[2,3]

[1]Geneva Observatory, University of Geneva, Sauverny, Switzerland
email: steven@stevenrieder.nl

[2]School of Physics and Astronomy, University of Exeter, Exeter, United Kingdom

[3]Scottish Universities Physics Alliance (SUPA), School of Physics and Astronomy, University of St. Andrews, United Kingdom

Abstract. We present Ekster, a new method for simulating the formation and dynamics of individual stars in a relatively low-resolution gas background. Here, we use Ekster to simulate star cluster formation in two different regions from each of two galaxy models with different spiral potentials. We simulate these regions for 3 Myr to study where and how star clusters form. We find that massive GMC regions form more massive clusters than sections of spiral arms. Additionally we find that clusters form both by accreting gas and by merging with other proto-clusters, the latter happening more frequently in the denser GMC regions.

Keywords. star cluster formation, star formation modeling

1. Introduction

Stars form in galaxies, from collapsing molecular clouds (Lada and Lada 2003). We see this happen mostly on the scales of individual Giant Molecular Clouds (GMCs) or molecular cloud complexes and the arms of spiral galaxies.

Simulations of star clusters generally focus on either starting from a single cloud (e.g. Bate et al. 2003), or take a distribution of stars as their starting point (e.g. Aarseth 1974). Such simulations either ignore the galactic environment completely, or include it only in rudimentary form, e.g. as a galactic tidal field.

Ideally, to simulate the formation of star clusters self-consistently one would run a full galaxy simulation with enough resolution to form individual stars. Computational limits make this unfeasible. Recently approaches have been made to more fully represent stellar populations with individual star particles (e.g. Wall et al. 2019) even if the gas resolution is not correspondingly high. These allow for studying the dynamics of the stars and the gas simultaneously.

We use `AMUSE`(Portegies Zwart and McMillan 2018) to combine SPH with multi-scale N-body dynamics and stellar evolution in a new simulation method, which we name `Ekster`. With this method we can simulate the formation of individual stars, while it also allows us to take the galactic environment into account.

Here, we follow cluster formation with full N-body dynamics. We start our simulations by extracting gas form a section centred on a GMC and a section of a spiral arm. We do this using two different spiral galaxy models, with different strength spiral arms, as a means of examining the role of spiral arms.

2. The Ekster method

We design our method `Ekster`†(Rieder and Liow 2021) to combine an SPH simulation at relatively low resolution with a method to form individual stars from star forming regions ("sinks") and dynamically evolve these. `Ekster` employs `AMUSE` as the environment that combines these elements. We use `Phantom` (Price et al. 2018) for gas hydrodynamics, `Petar` (Wang et al. 2020) for stellar dynamics and `SeBa` (Portegies Zwart and Verbunt 1996) for stellar evolution. We couple the gravitational dynamics between stars and gas using `Bridge` (Portegies Zwart et al. 2020), using a global timestep of 0.0025 Myr.

2.1. *Gas*

Gas particles in `Phantom` are integrated on individual time steps, while a synchronisation timestep of half the global timestep is used. All gas particles in Phantom have an equal mass (here: $1M_\odot$ per particle). When a star formation region forms, gas particles accreted by this region are removed from `Phantom`.

2.2. *Star formation*

When gas reaches a density of (10^{-18}g cm^{-3} and passes additional checks following the method in Price et al. (2018, paragraph 2.8.4), a sink particle will form and accrete all gas particles within a radius of 0.25 parsec (similar to the method in Wall et al. (2019)). This will accrete approximately $200M_\odot$, enough to probe the IMF without a dearth of high-mass stars. The position and velocity of the sink particle are taken as the centre-of-mass and centre-of-mass-velocity of the gas particles, while the velocity dispersion of the gas is also saved as a property of the sink. This sink will then start forming stars by drawing a random mass from a Kroupa (2001) initial mass function, creating a star only if its mass is still higher than the mass of the star. The new star will be placed at a random position within the accretion radius with a velocity drawn from a Gaussian distribution centred on the velocity dispersion of the sink, and its mass is subtracted from the sink's mass. This process continues until the sink no longer has enough mass to form the next star.

2.3. *Stars*

Once stars have formed, they are added to both the stellar evolution and stellar gravity modules. Stellar gravity is integrated using a combined tree/direct N-body method, with additional support for algorithmic regularisation to integrate binary stars. Stars are integrated without any softening, allowing for the dynamical formation of binary stars.

3. Simulations

Our initial conditions are based on snapshots from each of two galaxy scale simulations, one of which is the simulation shown in Dobbs and Pringle (2013). The other is identical apart from the stronger spiral potential, and ran to provide initial conditions for this work.

From each simulation, we take two regions. One region, which we denote 'cloud', centres on a massive GMC, whilst the other region, which we denote 'arm', centres on a section of spiral arm with a number of lower mass clouds. Thus we have two 'arm' regions, one in each simulation and two 'cloud' regions, again one in each simulation.

† publicly available at `https://github.com/rieder/ekster`

https://doi.org/10.1017/S1743921322001892 Published online by Cambridge University Press

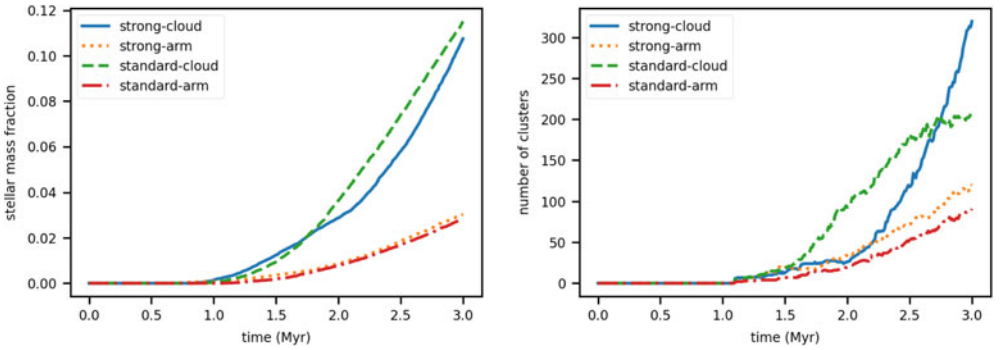

Figure 1. Left: Stellar mass fraction over time in the four simulations. Right: The number of clusters formed in the different models over time.

We use the two different models to investigate how cluster formation depends on the different galaxy models, and the different morphologies of the GMCs which form.

3.1. *Running the simulation*

After selecting the particles in our regions of interest, we re-sample the SPH particles following the method in Bending et al. (2020). Each original particle is split into 311 new particles of $1M_{\odot}$ each.

We run simulations of each of these regions with `Ekster`, using isothermal gas at 30 K. To preserve the large-scale environment of the original galactic simulation, we include the same tidal field used in the galaxy simulations.

Since our simulations do not include feedback, we limit our simulations to the embedded phase of star cluster formation, i.e. up to 3 Myr (Lada and Lada 2003). We save a snapshot every 0.01 Myr.

4. Results and discussion

We find that in all four simulations, star formation starts after $\sim$ 1 Myr (Figure 1, left panel). Both of the 'strong' models produce more clusters than their 'standard' equivalent by 3 Myr (Figure 1, right panel). Star formation is strongest in the 'cloud' regions of each simulation, but there is not a great difference between either the 'cloud', or the 'arm', regions from the 'strong' and 'standard' simulations. For the 'cloud' simulations, over 10% of the gas is converted to stars, whereas in the 'arm' regions it is around 3%, although we would expect that feedback may decrease these numbers.

In Figure 2 we show images of the column density of the four models in the final snapshot, with an inset showing the most massive cluster in each simulation. As expected, in the 'cloud' models stars have formed primarily towards the centre of the clouds, in what appears by eye to be more massive clusters. In the 'arm' models, clusters are more spread out along the total length of the arm. By eye, there is little obvious difference between the 'strong' and 'standard' models.

4.1. *Cluster evolution over time*

We compare the evolution of the four largest star clusters between similar regions in the two galaxies, as well as between different regions in the same galaxy. Figure 3 shows that cluster masses in the 'cloud' models grow to considerably larger values than in the 'arm' models.

https://doi.org/10.1017/S1743921322001892 Published online by Cambridge University Press

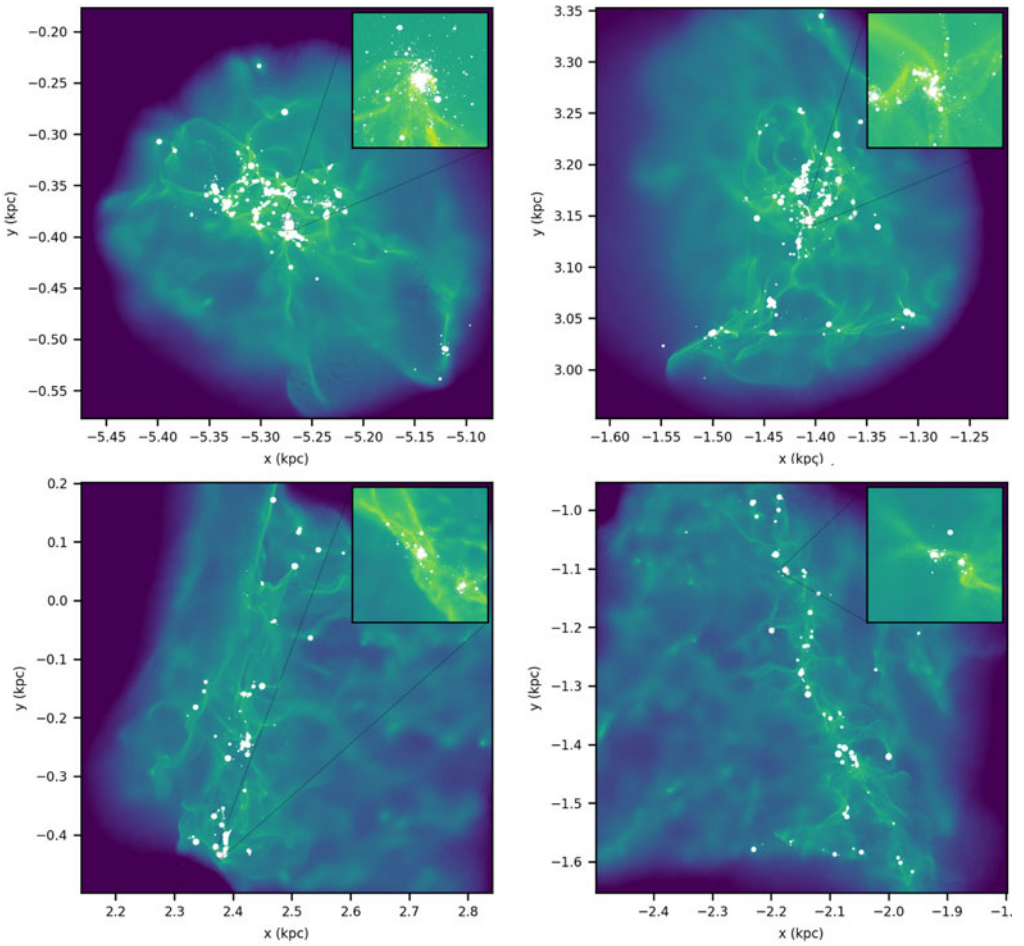

Figure 2. The four regions are shown at 3 Myr. The inset regions are 10 parsec wide and zoom in on the largest star cluster of each simulation. Top row: strong-cloud (left) and standard-cloud (right). Bottom row: strong-arm (left) and standard-arm (right).

Initially, the mass of the clusters increases linearly, indicating a steady conversion of gas into stars. Mergers of clusters happen more frequently in the 'cloud' simulations than the 'arm' simulations.

In the 'arm' simulations, growth slows down for most clusters after $\sim$1Myr, while in the 'cloud' simulations clusters continue to grow. This is caused by the stars having used up all the gas in their surroundings or because the stars have decoupled from the gas. In the 'cloud' simulations, this decoupling seems to not take place and as a result the clusters can grow larger.

4.2. *Cluster properties*

In Figure 4 we plot the cluster mass versus the half-mass radii, again at 3 Myr. Generally there is not a strong dependence of radius versus mass, as seen in observations (Portegies Zwart et al. 2010), though it is consistent with the relation in Marks and Kroupa (2012, eq. 7). We also show the young massive clusters Portegies Zwart et al. (2010, and references therein) plotted for comparison as open circles, which are similarly aged to our clusters ($<= 3.5$ Myr). We see again that the

https://doi.org/10.1017/S1743921322001892 Published online by Cambridge University Press

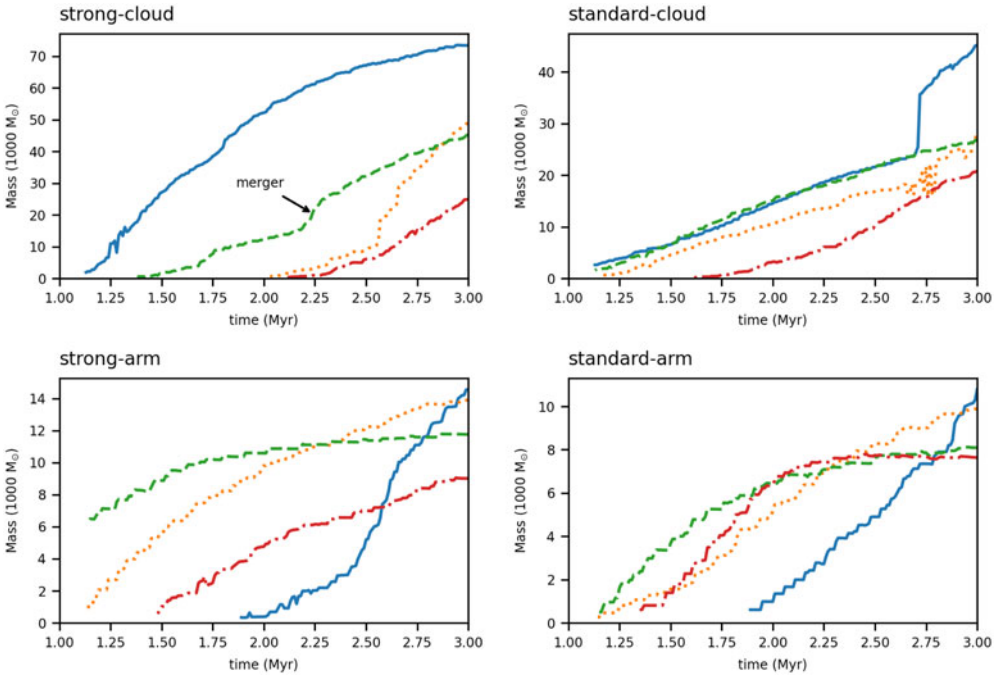

Figure 3. The mass of the four largest clusters from the four different simulations. Top left (green line) indicates an example of a merger. Wiggles in the orange line from the top right figure originate from a similar merger where the two progenitors have similar mass.

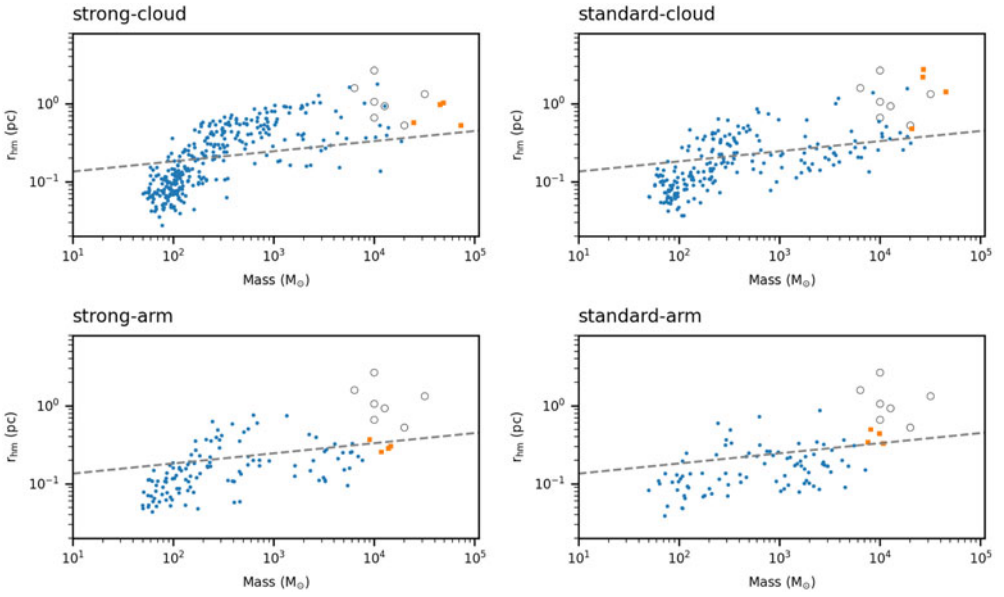

Figure 4. Mass versus half-mass radius for clusters at 3.0 Myr. The most massive clusters (orange squares) have properties comparable to the similarly aged observed young massive clusters (open circles). The dashed line indicates the relation from Marks and Kroupa (2012, Eq. 7).

https://doi.org/10.1017/S1743921322001892 Published online by Cambridge University Press

'cloud' regions produce more massive star clusters than the 'arm' regions. When comparing our simulated clusters to the observed ones, we find that the more massive of our clusters have similar masses and half-mass radii.

5. Conclusions

We have simulated the formation of star clusters using the `Ekster` method that combines high-precision N-body dynamics with SPH and stellar evolution. By comparing two GMC regions and two spiral arm regions from two different galaxies, we find that the GMCs are able to form larger star clusters in a shorter time compared to typical molecular clouds. This is independent of the galaxy scale simulation.

We also find that clusters partially grow by merging with other (proto-)clusters. We find that our more massive clusters have similar properties to observed young massive clusters, including a fairly constant mass radius relation.

Acknowledgements

SR acknowledges funding from STFC Consolidated Grant ST/R000395/1 and the European Research Council Horizon 2020 research and innovation programme (Grant No. 833925, project STAREX). CLD acknowledges funding from the European Research Council for the Horizon 2020 ERC consolidator grant project ICYBOB, grant number 818940.

References

S. J. Aarseth. *A&A*, 35(2):237–250, Oct. 1974.
M. R. Bate, I. A. Bonnell, and V. Bromm. *MNRAS*, 339(3):577–599, Mar. 2003.
T. J. R., Bending, C. L., Dobbs, and M. R. Bate. *MNRAS*, 495(2):1672–1691, June 2020.
C. L. Dobbs and J. E. Pringle. *MNRAS*, 432(1):653–667, Jun 2013.
P. Kroupa. *MNRAS*, 322(2):231–246, Apr 2001.
C. J. Lada and E. A. Lada. *ARA&A*, 41:57–115, Jan. 2003.
M. Marks and P. Kroupa. *A&A*, 543:A8, July 2012.
S. Portegies Zwart and S. McMillan. 2514-3433. IOP Publishing, 2018. ISBN 978-0-7503-1320-9. URL http://dx.doi.org/10.1088/978-0-7503-1320-9.
S. Portegies Zwart, I. Pelupessy, C. Martínez-Barbosa, A. van Elteren, and S. McMillan. *Communications in Nonlinear Science and Numerical Simulations*, 85:105240, June 2020.
S. F. Portegies Zwart and F. Verbunt. *A&A*, 309:179–196, May 1996.
S. F. Portegies Zwart, S. L. W. McMillan, and M. Gieles. *ARA&A*, 48:431–493, Sep 2010.
D. J. Price, J. Wurster, T. S. Tricco, C. Nixon, S. Toupin, A. Pettitt, C. Chan, D. Mentiplay, G. Laibe, S. Glover, C. Dobbs, R. Nealon, D. Liptai, H. Worpel, C. Bonnerot, G. Dipierro, G. Ballabio, E. Ragusa, C. Federrath, R. Iaconi, T. Reichardt, D. Forgan, M. Hutchison, T. Constantino, B. Ayliffe, K. Hirsh, and G. Lodato. *Publ. Astron. Soc. Australia*, 35:e031, Sep 2018.
S. Rieder and K. Y. Liow, Sept. 2021. URL https://doi.org/10.5281/zenodo.5520944.
J. E. Wall, S. L. W. McMillan, M.-M. Mac Low, R. S. Klessen, and S. Portegies Zwart. *ApJ*, 887(1):62, Dec. 2019.
L. Wang, M. Iwasawa, K. Nitadori, and J. Makino. *MNRAS*, 497(1):536–555, Sept. 2020.